Eur. Phys. J. Special Topics **222**, 1035–1046 (2013)

DOI: 10.1140/epjst/e2013-01904-2

THE EUROPEAN PHYSICAL JOURNAL SPECIAL TOPICS

Regular Article

Modeling of dynamics of field-induced transformations in charge density waves

T. Yi[1,3], N. Kirova[2,4,a], and S. Brazovskii[1,4]

[1] CNRS, LPTMS, URM 8502, Univerisité Paris-sud, 91405 Orsay, France
[2] CNRS, LPS, URM 8626, Univerisité Paris-sud, 91405 Orsay, France
[3] Departement of physics, South University of Science and Technology of China, Shenzhen, Guangdong 518055, China
[4] International Institute of Physics, 59078-400 Natal, Rio Grande do Norte, Brazil

Received 18 March 2013 / Received in final form 12 May 2013
Published online 15 July 2013

Abstract. We present a modeling of stationary states and their transient dynamic for charge density waves in restricted geometries of realistic junctions under the applied voltage or the passing current. The model takes into account multiple fields in mutual nonlinear interactions: the amplitude and the phase of the charge density wave complex order parameter, distributions of the electric field, the density and the current of normal carriers. The results show that stationary states with dislocations are formed after an initial turbulent multi-vortex process. Static dislocations multiply stepwise when the voltage across or the current through the junction exceed a threshold. The dislocation core forms a charge dipole which concentrates a steep drop of the voltage, thus working as a self-tuned microscopic tunnelling junction. That can gives rise to features observed in experiments on the inter-layer tunneling in mesa-junctions.

1 Introduction

Electronic crystals are a common form of space organization in conducting solids (see [1,2] for the recent collection and the latest review). They take forms of Wigner crystals at hetero-junctions and in nano-wires, charge density waves (CDW) in chain compounds, spin/charge density waves and charge-ordered ferroelectric states in organic conductors, stripes in doped oxides and cuprates. The CDW is a particular kind of electronic crystal which is most accessible experimentally and best treatable theoretically. It is a crystal of singlet electronic pairs, which frequently is formed in quasi one-dimensional (1D) conductors. Usually, the CDW amplitude A is small, then the electronic density and the associated lattice deformation are nearly sinusoidal $\sim A\cos(Qx+\varphi)$. This gives rise to the complex order parameter $\Psi = A\exp(i\varphi)$ which, together with similarities of opening gaps 2Δ in electronic spectra, allows for fruitful comparison with superconductors. The arbitrary chosen phase φ characterizes

[a] e-mail: kirova@lps.u-psud.fr

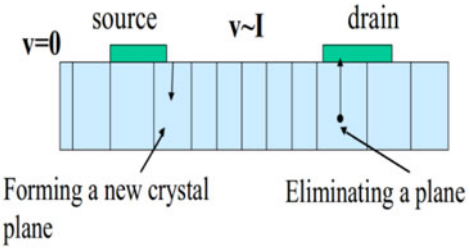

Fig. 1a. Dynamic origin for formation of dislocations in the course of the CDW sliding. Vertical lines indicate new crystal planes with dislocations being the leading edges of penetrating planes. Resulting elastic deformations can be measured by space-resolved X-ray diffraction as in Fig. 1b.

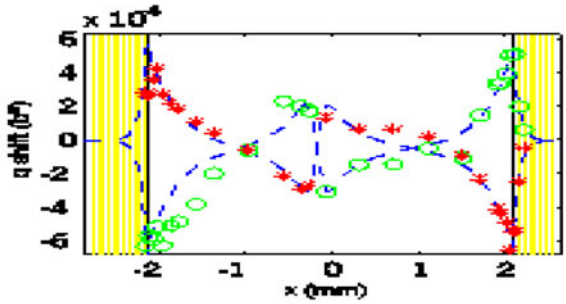

Fig. 1b. Visualization of phase-slips distribution by induced phase gradients having been measured as the local wave number shift of the sliding CDW [9]. Current conversion takes place near the junctions at x = ±2 mm and at the pseudo-junction near x ≈ 0 appearing due to a plane defect crossing the sample.

the ground state degeneracy while its distortions form the collective mode. Phase distortions are charged since the increment $\delta\varphi = \pm 2\pi$ adds/subtracts one CDW period, hence the charge ±2e (e is the electron's charge). Then the charge density (per unit length of one chain) is $n_c = e\varphi'/\pi$ where $\varphi' = \partial_x\varphi$ is the phase gradient along the chain.

Beyond the charged deformations, a main distinction of electronic crystals is that the number of unit cells is not fixed and it can be readjusted to absorb excess electrons or holes to the new extended ground state. Exchange of electrons with the CDW condensate goes on locally via topologically nontrivial deformations: discommensurations as domain walls, dislocations as vortices, solitons as anomalous quasi-particles. There are two origins for formation of such defects: dynamic and static ones.

The common dynamic scenario is related to the collective motion – the CDW sliding under the applied external electric field. To convert the injected normal current to the collective one and back, it is necessary to form additional crystal planes near the source contact and eliminate them near the drain one, see Fig. 1. The dislocations appear as leading edges of penetrating/retreating planes. One expects their transverse flow [3] in a thick channel, while plane phase slips can be more favorable in a wire [4–6]. The phase-slip events performed by the transverse flow of dislocations are distributed over a substantial length which has allowed for their identification by space-resolved synchrotron X-ray diffraction [7–9].

A static structure of topological defects can be formed in the CDW under applied transverse voltage or current [10] or under a surface strain [11]. The rigid CDW is an insulator in absence of normal carriers; then the applied potential 2V would not

be screened: $\Phi = 2\mathrm{Vy}/\mathrm{L}_y$ and the penetrating constant electric field $E = -2\mathrm{V}/\mathrm{eL}_y$[1] would cost the energy. Suppose nevertheless that the screening charge can come directly from the condensate density which requires for the charge penetration profile $\mathrm{n}_c(\mathrm{x},\mathrm{y}) \sim \partial_x\varphi$ in the transverse direction y. The interplay of the intra-chain elastic energy $\mathrm{W}_{elast} \sim (\partial_x\varphi)^2$ and of the Coulomb energy $\mathrm{W}_C \sim \Phi(\mathrm{y})\partial_\mathrm{x}\varphi$ tends to shift locally the equilibrium CDW wave number by $\partial\varphi_x \sim -\Phi(\mathrm{y})$ leading to the divergence of phases at different layers $\delta\varphi = \delta\mathrm{Qx} \sim -\Phi(\mathrm{y})\mathrm{x}$. Then the phases $\varphi(\mathrm{x},\mathrm{y}_m) = \varphi_m(\mathrm{x})$ on different chains m become non correlated and the energy of the long-range 3D ordering is lost growing linearly with x. This decoupling requires for a critical threshold voltage $\mathrm{V_t}$ which depends on the interlayer coupling energy J. Restoration of interlayer correlations goes via formation of topological defects – dislocations which will result in a vortex-like pattern for the CDW phase with the amplitude vanishing in the center.

2 Motivations from experiments

Tunneling experiments give an access to properties of electrons in solids by measuring transition rates (the current I(V)) between adjacent parts of the sample under the applied voltage V. Usually, the tunneling occurs between two different conductors across their hetero-junction or through a break of the same material. Here, we shall refer to a method of internal tunneling within a non-interrupted sample which is particularly effective in studies of strongly anisotropic (quasi two-dimensional or quasi one-dimensional) materials [12–15].

Usually it is supposed, being reasonably justified, that the formation of tunneling junction as well as applying voltage does not modify electronic states which are measured then as virgin ones. But the situation changes drastically in correlated systems showing a spontaneous symmetry breaking. There, the electronic spectra are formed self-consistently via interactions of electrons, or among them and the underlying lattice of the host crystal. Then the spectra and the very nature of states readjust to changes of a local concentration of electrons and even to individual particles.

Figure 2a below shows some representative results which interpretation allows identifying simultaneously: the traditional passive measurements of the single-particle excitations, the spectrum from the anomalous particle – the soliton, and the effect of the junction reconstruction under the applied field. Figure 2b amplifies the reproducible oscillations seen at and above the low threshold $\mathrm{V_t}$ of the Fig. 2a.

There are following important observations from Figs. 2a,b and other studies [12–15]:

- Apart from the expected peak at the CDW gap $\mathrm{V_g} = 2\,\Delta$, a much lower sharp threshold voltage $\mathrm{V_t} \approx 0.2\Delta$ is necessary for the tunneling onset.
- The ratio $\mathrm{V_t}\,(\mathrm{T})/\Delta\,(\mathrm{T}) \approx 0.2$ is temperature independent and nearly universal for all measured CDW states.
- The threshold voltage $\mathrm{V_t} \approx 1.3\mathrm{k_B}\,\mathrm{T_{CDW}}$ is linearly related with the temperature $\mathrm{T_{CDW}}$ of the 3D ordering for various CDW states. The threshold voltage might be accompanied by the phase decoupling of CDWs in adjacent layers which energy determines the T_{CDW}.
- The pair-breaking peak magnitude 2Δ is not multiplied by $\mathrm{N} \sim 20$–30 – a number of layers in the junction: the tunneling seems to be concentrated at just one elementary interval. Contrarily, in similar devices for superconductors the peak appears at $\mathrm{V} = 2\,\Delta \times \mathrm{N}$ [12,13].

[1] Here and below, the definitions of electric potential and applied voltage include the electron's charge e.

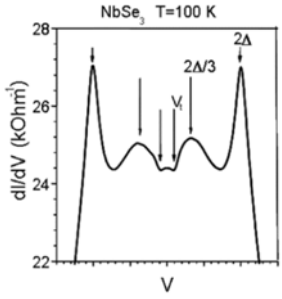

Fig. 2a. Differential conductance dI/dV as a function of the voltage V normalized to the CDW gap – for the upper CDW in $NbSe_3$. [12,13]. We identify: the absolute threshold at low $V_t = 0.2\Delta$, the amplitude soliton at the expected $E_{AS} \approx 2\Delta/3$, the inter-gap energy 2Δ for creation of the e – h pair.

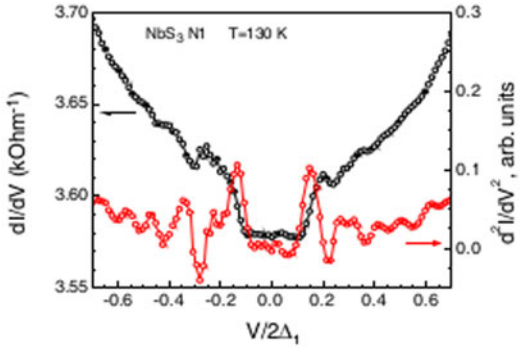

Fig. 2b. Fine structure in the differential conductance dI/dV and the second derivative $d^2\,I/dV^2$ as seen near the threshold voltage for the upper CDW in $NbSe_3$ at T = 130 K [15]. Similar features appeared also for the lower CDW in $NbSe_3$; the threshold at V_t was clearly seen also in TaS_3.

3 Qualitative theory: From a lattice of solitons to an arrays of dislocations

3.1 Discommensurations in a two-layers model

A minimal model for the inter-layer decoupling takes into account only two layers kept at potentials $\pm V$. The energy functional W can be written as

$$w = \int dx \left\{ \frac{\hbar \nu_F}{4\pi} \left[\left(\frac{d\varphi_1}{dx} \right)^2 + \left(\frac{d\varphi_2}{dx} \right)^2 \right] + \frac{V}{\pi} \left(\frac{d\varphi_1}{dx} - \frac{d\varphi_2}{dx} \right) - J \cos(\varphi_1 - \varphi_2) \right\}. \tag{1}$$

Its minimization allows for the lattice of discommensurations which develop starting from an isolated $2\,\pi$ soliton in difference of phases:

$$\varphi\,(x) = \varphi_2\,(x) - \varphi_1(x) = 2\mathrm{Arccos}(\tanh(x/l)) \quad l \propto J^{-1/2}. \tag{2}$$

The soliton energy $E_s \sim (\hbar v_F J)^{1/2}$ is identified as a critical voltage V_{cr}. Here v_F is the Fermi velocity in the parent metal, J is the interlayer coupling. At $V > V_{cr}$ the solitons form the lattice and finally they overlap at $V \gg V_{cr}$ when the phase difference changes

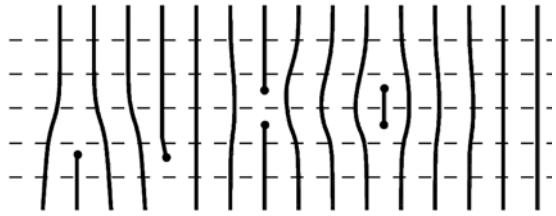

Fig. 3. From left to right: the positive dislocations as the leading edge, the negative dislocation, the $\pm 2\pi$ on-chain solitons as dipoles of dislocations. Solid lines – fronts of CDW maxima, dashed lines – chains.

nearly linearly φ_1-$\varphi_2 \approx 2Vx/\hbar \mathrm{v_F}$ which means the complete decoupling. The charge redistribution between planes forms the double layer which provides a sharp potential drop concentrated within the soliton length, hence forming a tunneling junction.

3.2 Continuous model: From discommensurations to dislocations

The above model of two planes was only a transparent illustration of decoupling under the applied voltage. In reality, there is a bulk of many planes with a voltage difference monitored at its sides, while the decoupling happens somewhere in-between. The former lattice of discommensurations must be generalized to a sequence of dislocation lines (DL), see Fig. 3.

The critical voltage is identified as the DL entry energy, in some analogy to the $\mathrm{H_{c1}}$ field in superconductors. Following a plane just above the decoupled spacing, the sequence of DLs will look almost like the solitonic lattice. But along more distant planes the discommensurations become more and more spread, until they overlap to become ill noticed. One can keep track of that thanks to the notion of dislocations and their arrays. Remind that the DL in the CDW [16,17] is a topological defect such that going around it we acquire or lose one period – for the CDW it is the vortex phase increment $\delta\varphi = \pm 2\,\pi$.

Bypassing the DL at the origin by some two paths along x – one above $y > 0$ and another below $y < 0$, this phase increment is recovered. Near the dislocation core the phase gradients diverge grad $\varphi \longrightarrow \infty$, hence the CDW amplitude vanishes A $\longrightarrow 0$.

Instead of the two-planes interaction, Eq. (1), now there is a distributed shear energy

$$-\int dx J\cos\left(\varphi_1-\varphi_2\right) \to \frac{\hbar v_F}{4\pi}\beta^2\int dx\,dy\left(\partial_y\varphi\right)^2, \quad \beta^2 \sim \frac{Jd_y}{\hbar v_F} \ll 1$$

where β is the dimensionless anisotropy parameter, $\mathrm{d_y}$ is the distance between planes. Phase variations in the chain direction x, being charged, become particularly costly in the Coulomb energy; hence they must be very slow in comparison with variations in the inter-chain direction y. Then the deformations and the electric field, concentrated over characteristic lengths $\mathrm{L_y}$ and $\mathrm{L_x}$, forming a thin ($\mathrm{L_y} \ll \mathrm{L_x}$) and long (over the whole length $\mathrm{L_z}$ in z direction) stripe. Since, by the DL definition, the phase changes by $\pm\pi$ while going along the x axis at any level y, then the stripe is a double-layer of charges $\pm \mathrm{eL_x}L_z/\mathrm{s}$ and the capacitance is the one of a plane condenser: $\mathrm{L_z}\,L_\mathrm{x}/L_\mathrm{y}$. Then the Coulomb energy is

$$\mathrm{W_C} \sim \frac{\left(\mathrm{eL_yL_z/s}\right)^2}{\mathrm{L_xL_z/L_y}} \sim \frac{\hbar \mathrm{v_F}}{\mathrm{r_0^2}}\frac{\mathrm{L_zL_y^3}}{\mathrm{L_xs}}, \quad 1/r_0^2 = 8e^2/\epsilon\hbar v_F s$$

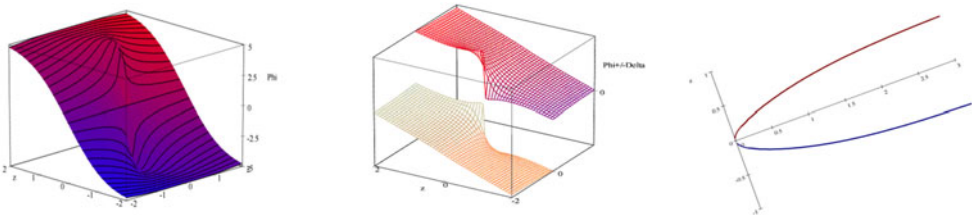

Fig. 4. Illustration of the voltage drop at the vortex core for a single dislocation (left); 3D plot (center) and the contour plot (right) for surfaces $\Phi(\mathrm{x},\mathrm{y}) = \pm\Delta$ between which the tunnelling takes place. The plots were made with analytical formulas [18] adjusted to a bounded system.

where r_0 is the short Tomas-Fermi length of the parent metal, $\mathrm{s} = \mathrm{d_y d_z}$ is the unit area per one chain. The shear energy is

$$W_{shear} = L_z \frac{\hbar \mathrm{v_F}}{d_y d_z} \frac{\beta^2}{4\pi} \int dx \;\; dy \; (\partial_y \varphi)^2 \sim \frac{\hbar \mathrm{v_F} \beta^2 \mathrm{L_x} L_z}{\mathrm{L_y} s}.$$

Notice that the usual compression energy $\mathrm{W_{compr}}$ is negligibly small in comparison with the Coulomb energy $\mathrm{W_C}$:

$$W_{\mathrm{compr}} = L_z \frac{\hbar \mathrm{v_F}}{4\pi s} \int dx \;\; dy \; (\partial_x \varphi)^2 \sim \frac{\hbar \mathrm{v_F} \mathrm{L_y} L_z}{\mathrm{s L_x}}$$

and we shall not take it into account. From minimization of the total energy

$$W_{tot} = W_C + W_{shear}$$

over the scale L_x at a given scale L_y we obtain

$$L_x = \frac{L_y^2}{\beta r_0}, \quad W_{tot} = \Phi_0 \;\; M, \quad \Phi_0 = \pi \beta \hbar \frac{\mathrm{v_F}}{\mathrm{r_0}}.$$

Here $\mathrm{M} = \mathrm{L}_y \mathrm{L}_z/\mathrm{s}$ is the number of chains crossing the path of the DL while it was submerging to the depth L_y. These simple estimations recover new scales: Φ_0, $\mathrm{d} = \beta \mathrm{r_0}$, and the parabolic shape $\mathrm{L}_x \sim \mathrm{L}_y^2/\mathrm{d}$ ($d \sim 1$ Å is very small).

Coulomb interaction increases the energy cost to create the DL, but the same time it empowers the efficiency of building the electric field. The potential jump Φ_0 is concentrated in a very narrow region near a dislocation line, within the single spacing $\mathrm{y_{core}} \sim \mathrm{d_y}$ if we come as close as $\mathrm{x}_{core} \sim \mathrm{d}_y^2/\mathrm{d} \sim 10\,\mathrm{nm}$ which is still a rather wide spot. Away from the core, at a distance X along the chains, the same increment requires for progressively larger width $\mathrm{Y} \sim (\mathrm{Xd})^{1/2}$ (see Fig. 4). Near the DL core the potential drops just between the nearest planes which provides an efficient tunneling. Away, the tunneling must proceed through the number $\mathrm{Y/d}_y \sim (\mathrm{X/x}_{core})^{1/2}$ of stacks). Hence this is the grid of dislocation lines which determines the tunneling; their growing number will affect the growth of I(V) above the threshold. Ideally, the jumps will be observed when a new DL enters the junction.

There may be more measurable features related to mid-gap states produced by the DL's cores. Indeed, the phase-only descriptions of the DL resembles the Josephson vortices in layered superconductors which do not need a normal core.

Proliferation of the DL from an interplane spacing to the next one requires for capturing pairs of electrons or holes. But capturing only one particle advances the elementary segment of the DL by half of the period; that is to the conduction plane

where the normal core is necessary. This requirement meets perfectly the CDW property that its state with one unpaired electron is the amplitude soliton where the CDW amplitude passes through zero. Such an amplitude soliton has been recently observed indeed in STM experiments [19,20]. The energy of the amplitude soliton (theoretically $E_{AS} = 2\Delta/\pi$) must be paid for proliferating of an elementary segment of the dislocation line which can be one of observed tunneling features [14] (the lower peak in Fig. 2a). Also, the amplitude deformation creates the mid-gap state, accommodating the unpaired electron, which can add a new spectroscopic feature in optics or STM.

4 The model for simulations

Above estimations and qualitative conclusions are supported by analytic results [10, 18] for the phase-only description $A \equiv 1$ which is valid sufficiently far away from the vortex core. Accessing the vortex core with its expected node of the amplitude and account of screening by normal carriers could be achieved by a numerical minimization of the total energy [21]. But the actual experimental situation corresponds not to static but at best stationary states where the electric field is brought in by currents of normal currents; that requires for solutions of coupled systems of partial differential equations. Finally, very interesting dynamic effects take place during the initial transient stage, and that requires for more complicated time dependent modeling presented below and, for other regimes, in [21–23].

We have performed the numerical modeling of static, stationary and transitory effects in CDW keeping in mind the following goals:

- To allow for creation of dislocations without seeding them or promoting in any way.
- To work in a realistic constrained geometry.
- To use experimentally realistic parameters and justified equations.

The model should take into account multiple fields in mutual nonlinear interactions: the phase φ and the amplitude A of the CDW order parameter $\Psi = Ae^{i\varphi}$, distributions of the electric potential Φ, of the density n and the current j of normal carriers. All variables are functions of two coordinates and the time (x,y,t).

We describe the CDW dynamics within the dissipative time dependent Ginsburg-Landau like approach. The static state is determined by minimum of the total energy functional $W = W_{CDW} + W_{el}$. Here, the energy of the CDW condensate W_{CDW} has a form:

$$W_{\mathrm{CDW}} = \int d^3r \left\{ \frac{\Delta\xi}{4\pi s} \left[\left| \frac{\partial\Psi}{\partial x} \right|^2 + \beta^2 \left| \frac{\partial\Psi}{\partial y} \right|^2 \right] + \frac{\Delta}{2\xi s} |\Psi|^2 \ln \frac{|\Psi|^2}{e} \right\}, \quad \xi = \frac{\hbar v_{\mathrm{F}}}{\Delta}.$$

Here Δ is the CDW energy gap in equilibrium, ξ is the correlation length. In the phase-only limit, the first two terms describe elastic deformations – the compression and the share. The third one is the CDW ground state energy with the minimum at $A = |\Psi| = 1$.

W_{el} is the energy of the electric field and of free carriers:

$$W_{el} = \int d^3r \left[\frac{\Phi}{s} \frac{A^2}{\pi} \frac{\partial\varphi}{\partial x} + \frac{\Phi n(\varsigma)}{s} - \frac{\varepsilon}{8\pi} |\nabla\Phi|^2 + F(n) \right], \quad \varsigma = \frac{\partial F}{\partial n} \tag{3}$$

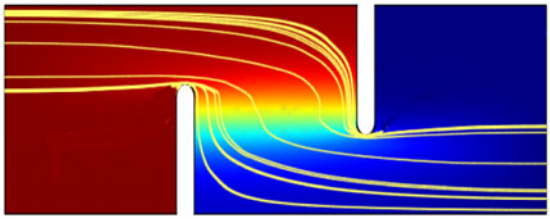

Fig. 5a. The real geometry of the overlap junction and distributions of the electrochemical potential $\mu = \varsigma + \Phi$ (the density) and the normal current (the lines) below the threshold for appearance of dislocations.

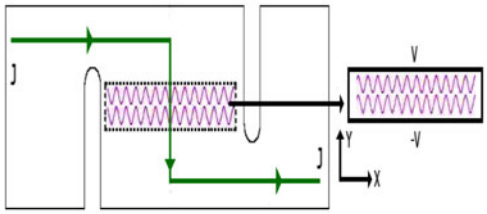

Fig. 5b. Selection for the modeling of the active rectangular central part where stationary vortices will stay. The arrows indicate the mean current flow. Wavy lines remind about the oscillating CDW.

where $\varepsilon \sim 10$ is the host dielectric constant. The first and the second terms in W_{el} describe the interaction of collective and normal charges with the electric field; the third term is the field energy. The last term F(n) is the free energy of normal carriers and ς(n) is their local chemical potential.

The evolution is governed by dissipative equations:

$$-\gamma_A \frac{\partial A}{\partial t} = \frac{\delta W}{\delta A} \quad -\gamma_\varphi \frac{\partial \varphi}{\partial t} = \frac{\delta W}{\delta \varphi} \quad \frac{\delta W}{\delta \Phi} = 0 \quad \nabla j + \frac{\partial n}{\partial t} = 0 \tag{4}$$

where $\gamma_{A,\varphi}$ are the damping coefficients. The parameter γ_φ is related with the experimentally measured CDW collective conductivity σ_{CDW} as

$$\gamma_\varphi = \frac{\xi \Delta}{16\pi^2 s r_0^2} \frac{1}{\sigma_{\mathrm{CDW}}}.$$

The relaxation time for the amplitude A of the order parameter is much shorter than for the phase φ, so we can put $\gamma_A = 0$.

Unlike more conventional Ginzburg-Landau models, here there are two more equations: the Poisson equation for the electric potential which couples collective and normal charges, and the charge conservation law for diffusion of normal carriers. Details on equations and boundary conditions are given in the Appendix.

5 Results of modeling and discussion

A typical junction [14,15] is formed by two overlapping slits (see Fig. 5, left) which enforce the current to deviate to the transverse direction Y of high resistivity. That gives rise to the strong voltage drop at the central rectangle which can be considered as the most significant region. Hence here we shall study the simplified rectangular geometry (see Fig. 5, right) which provides a necessary intuition and also can be

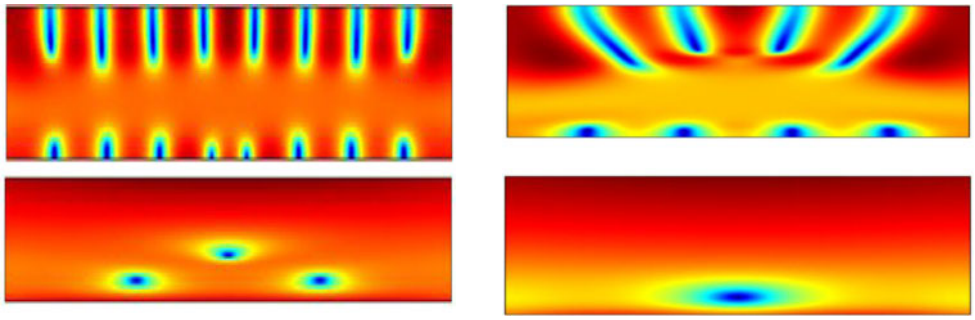

Fig. 6. CDW amplitude A in the vortex state, A changes from 1 in the bulk to zero in the core. The left and the right panels differ by parameters of geometry and structural anisotropy. Top plots are snapshots of the initial dynamic states where the order parameter maintains to be zero over the whole trace of the vortex cores. Bottom plots are the final stationary states with remnant stable vortices.

applied to other experiments with traditional field effect geometry. Results for the complete geometry with slits can be found elsewhere [22].

Two regimes with two types of dislocations have been revealed by the simulation: the fast moving dynamic vortex with a tail of zero amplitude and the slow or stationary vortex with the amplitude node only in its center. The transient regime starts at 10^{-11} sec (the limit of our dissipative approximation) and it lasts up to 10^{-8} sec. During this turbulent stage, dynamic vortices appear in large numbers at the upper and lower boundaries of the sample, see Fig. 6. Most of vortices annihilate with partners of opposite signs or disappear after sweeping between the boundaries. The remnant ones evolve into a small number of stationary vortices at a final stage.[2] By varying the junction height and/or the value of the anisotropy parameter from 0.1 to 0.01 we obtain different vortex configurations. The thresholds found in these situations are all of the order $\sim 10\,\mathrm{meV}$, but the final configurations are different, which might be due to interaction between the vortices. E.g. formation of a triangular vortex lattice for $\beta = 0.01$ at $\mathrm{V} = 15\,\mathrm{meV}$ is shown in Fig. 6, left panel; the right panel shows formation of a single vortex.

Figure 7 shows the 3D plot of the amplitude equivalent to the density plot of the Fig. 6 (bottom right). We see a general suppression of the amplitude over the sample median and then the strong deep down to $\mathrm{A} = 0$ in the middle. The phase, which contours are shown in the basal plane, rotates by 2π around the point of the zero amplitude thus proving that this is the vortex center.

The vortex core strongly perturbs the electric potential Φ and the concentration of normal carries (seen via their chemical potential ς) as shown in Fig. 8. These strong variations are in general accord with the above qualitative discussion and estimations, but the actual picture is more complicated showing the non monotonous double-hump shape of Φ.

The strong drop of the electric potential Φ and the accumulation of the carriers' density are concentrated near the vortex core indicating the location of tunneling processes. This result is in accordance with the above presented analytic results for a static dislocation in linear approximation for the infinite media. The increased tunneling probability near the core explains the observed sequence of peaks in Fig. 2.

[2] The generated movies can be found supplementary at web site links [24].

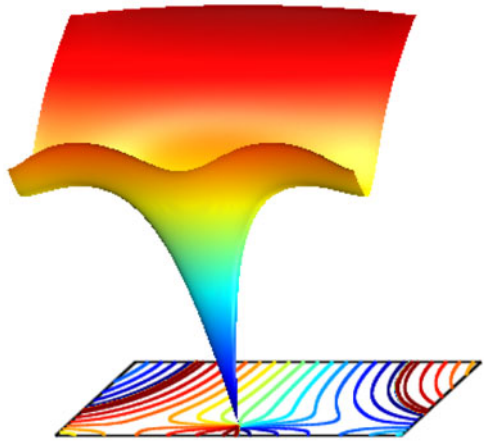

Fig. 7. The 3D plot of the amplitude for the single-vortex final state. The basal plane gives the contour plot of the phase which acquires the 2π increment by going around the point with A = 0.

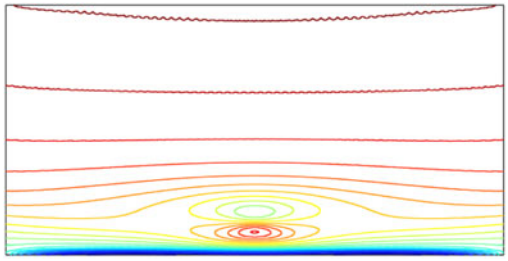

Fig. 8a. Contour plot of the electric potential $\Phi(x, y)$.

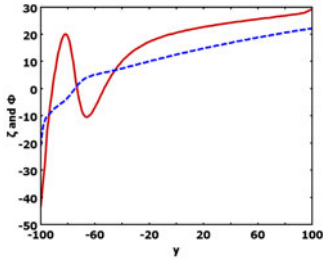

Fig. 8b. Plots of $\Phi(0, y)$ (red solid line) and the chemical potential $\varsigma(0, y)$ (blue dashed line, 10 times reduced) along the vertical line x = 0 crossing the vortex core.

6 Conclusions

Charge density waves are typical symmetry broken states in low-dimensional conductors. They attract much attentions in many studies presented at the IMPACT meeting and in this volume. The CDW is a particular kind of electronic crystals; as such, it possesses the dislocations – in some analogy to vortices in superconductors. In dynamics, the sweeping of dislocations across conducting chains serves as a phase-slip phenomenon providing the conversion of excess normal carriers to the condensed ones. Static dislocations appear as the ground state reconstruction of a junction when the electric field or the normal current are applied in the transverse direction.

Appearance of mismatch topological defects can be common to field-effect [25,26], electrostatic and optical [27] ways of doping. In all cases, the impact perturbation decays in depth of the sample thus passing through critical values for phase transformations.

We conclude that reconstruction in junctions of the CDW is a convenient playground for modern efforts of the field-effect and optical transformations in strongly correlated material with spontaneous symmetry breakings.

Appendix. Detailed equations and boundary conditions

The equations (4) for our modeling can be written as

$$\frac{\xi}{2}\nabla A^2\nabla\varphi + \frac{\partial}{\partial x}A^2\Phi = -\gamma_\varphi A^2\frac{\partial\varphi}{\partial t} \tag{A.1}$$

$$\frac{1}{2\pi}\left(\nabla^2 A + A(\nabla\varphi)^2\right) + \frac{1}{\xi^2}|A|\ln|A|^2 = -\gamma_A\frac{\partial A}{\partial t} \tag{A.2}$$

$$-\frac{\varepsilon s}{4\pi e^2}\nabla^2\vec{\mathbf{\Phi}} = \frac{1}{\pi}\frac{\partial\varphi}{\partial x} + n(\varsigma)\cdot \tag{A.3}$$

The system is completed by the diffusion equation for normal carriers which are characterized by the conductivity tensor $\sigma = (\sigma_{\mathrm{x}}, \sigma_{\mathrm{y}})$ (with a typical anisotropy $\sigma_{\mathrm{x}}/\sigma_{\mathrm{y}} \approx 100$):

$$\nabla j + \frac{\partial n}{\partial t} = -\nabla\left[\hat{\sigma}\nabla\left(\varsigma + \Phi\right)\right] + \frac{\partial n}{\partial t} = 0. \tag{A.4}$$

We suppose that the normal carriers occupy a 2D pocket with a small Fermi energy ε_{F} and a concentration n_0 in equilibrium at $\mathrm{T} = 0$, then

$$n(\varsigma) = \frac{n_0 T}{\varepsilon_F}\ln\left(1 + \exp\left(\frac{\varepsilon_F + \varsigma}{T}\right)\right)\cdot \tag{A.5}$$

The boundary conditions are as follows:

A. The normal CDW stress vanishes at the boundaries.

$$\left(\frac{\hbar v_{\mathrm{F}}}{2}A^2\nabla\varphi - A^2\Phi\vec{\boldsymbol{x}}\right)\cdot\vec{\boldsymbol{v}} = 0 \quad \nabla A\cdot\vec{\boldsymbol{v}} = 0. \tag{A.6}$$

B. The normal electric field vanishes at all boundaries

$$\Phi\cdot\vec{\boldsymbol{v}} = 0. \tag{A.7}$$

This choice corresponds to the total electro neutrality and ensures the full confinement of the electric field within the sample.

C. No normal current flow at the boundaries except for the two source/drain boundaries left for the applied voltage. There, the electro-chemical potentials are monitored:

$$\nabla\cdot\vec{\boldsymbol{v}}\left(\zeta + \Phi\right) = 0 \; or \; \zeta + \Phi = \pm V. \tag{A.8}$$

Above, $\vec{\boldsymbol{x}}$ and $\vec{\boldsymbol{v}}$ are the unit vectors along the chain and normal to the sample boundary.

References

1. Proceedings of the International Research School and Workshop on Electronic Crystals ECRYS 2011, Physcia B **407**, edited by S. Brazovskii, N. Kirova, P. Monceau (2011)
2. P. Monceau, Adv. Phys. **61**, 325 (2012)
3. N.P. Ong, K. Maki, Phys. Rev. B **32**, 6582 (1985)
4. L.P. Gor'kov, JETP Lett. **38**, 87 (1983)
5. L.P. Gor'kov, Sov. Phys. JETP **59**, 1057 (1984)
6. I. Batistic, A. Bjelis, L. Gor'kov, J. Phys. (France) **45**, 1049 (1984)
7. S.G. Lemay, M.C. de Lind van Wijngaarden, T.L. Adelman, R.E. Thorne, Phys. Rev. B **57**, 12781 (1998)
8. A.F. Isakovic, P.G. Evans, J. Kmetko, K. Cicak, Z. Cai, B. Lai, R.E. Thorne, Phys. Rev. Lett. **96**, 046401 (2006) and refs. therein
9. A. Ayari, R. Danneau, H. Requardt, L. Ortega, J.E. Lorenzo, P. Monceau, R. Currat, S. Brazovskii, G. Grübel, Phys. Rev. Lett. **93**, 106404 (2004) and refs. therein
10. S. Brazovskii, S. Matveenko, Sov. Phys. JETP **74**, 864 (1992)
11. N. Kirova, S. Brazovskii, J. Phys. IV (France) **131**, 147 (2005)
12. Yu.I. Latyshev, P. Monceau, A.P. Orlov, S.A. Brazovskii, Th. Fournier, Supercond. Sci. Technol. **20**, S87 (2007)
13. Yu.I. Latyshev, P. Monceau, S.A. Brazovskii, A.P. Orlov, T. Yamashita L.N. Bulaevskii, Phys. Stat. Sol. (c) **3**, 3110 (2006)
14. Y.I. Latyshev, P. Monceau, S. Brazovskii, A.P. Orlov, T. Fournier, Phys. Rev. Lett. **95**, 266402 (2005)
15. Y.I. Latychev, P. Monceau, S. Brazovskii, A.P. Orlov, T. Fournier, Phys. Rev. Lett. **96**, 116402 (2006)
16. D. Feinberg, J. Friedel, J. Phys. (France) **49**, 485 (1988)
17. D. Feinberg, J. Friedel, *Low-dimensional electronic properties of molybdenum bronzes and oxides* (Kluwer Academic Publisher, 1989), p. 407
18. S. Brazovskii, S. Matveenko, Sov. Phys. JETP **72**, 860 (1991)
19. S. Brazovskii, Ch. Brun, Zhao-Zhong Wang, P. Monceau, Phys. Rev. Lett. **108**, 096801 (2012)
20. Tae-Hwan Kim, Han Woong Yeom, Phys. Rev. Lett. **109**, 246802 (2012)
21. T. Yi, Y. Luo, A. Rojo-Bravo, N. Kirova, S. Brazovskii, J. Supercond. Nov. Mag. **25**, 1323 (2012)
22. T. Yi, Y. Luo, A. Rojo-Bravo, S. Brazovskii, Physica B **407**, 1839 (2012)
23. T. Yi, *Modeling of dynamical vortex states in charge density waves*, Ph.D. thesis, University Paris-Sud 11, 2012, `http://www.theses.fr/2012PA112200`
24. Movies after the modeling are available at `http://lptms.u-psud.fr/members/brazov/Slit1`, `http://lptms.u-psud.fr/members/brazov/Slit2`, `http://lptms.u-psud.fr/members/brazov/Rectangle`
25. N. Kirova, Curr. Appl. Phys. **6**, 97 (2006)
26. N. Kirova, IJHSES **17**, 172 (2007)
27. R. Yusupov, T. Mertelj, V.V. Kabanov, S. Brazovskii, J.-H. Chu, I.R. Fisher, D. Mihailovic, Nat. Phys. **6**, 681 (2010)